

Cite this: *RSC Adv.*, 2019, **9**, 9828

Received 10th January 2019
Accepted 23rd March 2019

DOI: 10.1039/c9ra00217k
rsc.li/rsc-advances

Facile synthesis of ordered mesoporous zinc alumina catalysts and their dehydrogenation behavior†

Ming Cheng,^{ab} Huahua Zhao,^a Jian Yang,^a Jun Zhao,^a Liang Yan,^a Huanling Song^{*a} and Lingjun Chou^a

Ordered mesoporous Zn/Al_2O_3 materials with varying Zn content were simply prepared via an evaporation-induced self-assembly (EISA) method. Dehydrogenation of isobutane to isobutene was carried out on these materials; an isobutane conversion of 45.0% and isobutene yield of 39.0% were obtained over the 10%Zn/ Al_2O_3 catalyst at 580 °C with 300 h⁻¹ GHSV. The obtained materials with Zn content up to 10% possess large specific surface area and big pore volume and zinc species can be highly dispersed on the surface or incorporated into the framework. The acidity of these catalysts was changed by the introduction of Zn, the decrease of strong acid sites is conducive to the promotion of isobutene selectivity and the weak and medium acidic sites played an important role in isobutane conversion. In addition, these catalysts exhibited good catalytic stability, due to the effective inhibition of coke formation by the ordered mesoporous structure.

1. Introduction

Isobutene is one of the most important raw materials and intermediates to produce butyl rubber, ETBE (ethyl *tert*-butyl ether), polyisobutene and other chemicals.^{1,2} To better fulfill the ever-increasing market demand, a small portion of its production is by isobutane dehydrogenation.³ Currently, Cr_2O_3/Al_2O_3 and Pt/Al_2O_3 are the two most common and employable catalysts in industrial production.^{4,5} However, some unavoidable drawbacks limit their further application, because Pt is expensive and has poor availability, while Cr is not environmentally-friendly due to its toxicity. Therefore, the exploitation of novel catalysts with superior catalytic properties, low cost and non-pollution for isobutane dehydrogenation is highly recommendable.^{6–8}

At present, all kinds of metal catalysts, such as vanadium-based, iron-based, molybdenum-based catalysts, have been widely investigated in this dehydrogenation reaction.^{9–12} In particular, owing to the excellent catalytic performance, Zn based catalysts have been interested and gazed considerably in the direct dehydrogenation of isobutane. For example, Zn modified HZSM-5 materials were found effective for activation of isobutane and high conversion obtained.^{13,14} Unfortunately,

the poor selectivity with respect to the formation of many undesired dry gas (CH_4 and C_2H_6) impeded its more broad applications, which probably derived from redundant strong acidic sites of HZSM-5 zeolite. Liu *et al.* reported that 27.5% isobutane conversion and 83.8% isobutene selectivity obtained in isobutane dehydrogenation over Zn/S-1 catalyst, because strong acid sites were absent.¹⁵ Moreover, Zn/Ti thin film and Zn/Ga oxide catalyst has also been referred in isobutane dehydrogenation.^{16,17}

Recently, ordered and adjustable mesoporous alumina materials have drawn research much attention. Coupled with their moderate surface acidity and good thermostability, ordered mesoporous alumina as heterogeneous catalyst support has a wonderful applying prospect.¹⁸ Morris *et al.* successfully synthesized $NiO-Al_2O_3$ composites with ordered mesoporous structure and the metal oxide well dispersed on the alumina support.¹⁹ Yuan *et al.* reported a simple route to synthesize $\gamma-Al_2O_3$ using P123 template agent, which have high quality mesoporous structure.²⁰ Schweitzer *et al.* put forward the computed minority catalytic pathway consists of undesired C–C bond cleavage at Zn(II) site had a significantly higher activation energy barrier and the high olefin selectivity observed for single-site Zn(II) on SiO_2 .²¹ In our previous work, well-ordered mesoporous Cr_2O_3/Al_2O_3 catalysts were synthesized and showed an advantage in catalytic stability.²² So far, almost no research was reported on ordered mesoporous zinc alumina composites for alkane dehydrogenation.

This study firstly prepared ordered mesoporous xZn/Al_2O_3 catalysts with different Zn content via evaporation-induced self-assembly (EISA) method and evaluated the catalytic performances in isobutane dehydrogenation. The textural properties

^aState Key Laboratory for Oxo Synthesis and Selective Oxidation, Lanzhou Institute of Chemical Physics (LICP), Chinese Academy of Sciences, Lanzhou 730000, PR China.
E-mail: ljchou@licp.ac.cn; songhl@licp.ac.cn

^bUniversity of Chinese Academy of Sciences, Beijing 100049, PR China

^cSuzhou Research Institute of LICP, Chinese Academy of Sciences, Suzhou 215123, PR China

† Electronic supplementary information (ESI) available. See DOI: [10.1039/c9ra00217k](https://doi.org/10.1039/c9ra00217k)

of obtained materials were characterized by XRD analysis, N₂ adsorption–desorption and TEM. And we also discussed the form of Zn species, metal-support interaction and surface acidity by XPS, H₂-TPR and NH₃-TPD. Besides, all the characterizations were associated with catalytic reactions.

2. Experimental

2.1. Catalyst preparation

Ordered mesoporous Zn/Al₂O₃ materials were prepared *via* EISA method according to the previous literatures.^{20,23,24} In a typical procedure, 1.0 g P123 as surfactant was added to 20 ml ethanol and the solution was stirred for 40 min, followed by the addition of a mmol aluminum isopropoxide, *b* mmol Zn(NO₃)₂·6H₂O (*a* + *b* = 10 mmol) and 1.6 ml nitric acid. After 6 h of stirring, the mixed solution was transferred to a culture dish and kept in drying oven at 60 °C for two days. The obtained xerogel was calcined at 600 °C for 5 h. The catalysts were denoted as *x*Zn/Al₂O₃, where the nominal molar ratio *x* = (*b*/*a* + *b*) × 100%.

2.2. Catalytic dehydrogenation

The direct dehydrogenation of isobutane was studied in fixed-bed quartz reactor. Typically, 900 mg of catalyst was sieved at 60–80 mesh. The reaction temperature was set at 560–620 °C. The reactant gas was fed by gas hourly space velocity (GHSV) of 300 h⁻¹. The composition of the gaseous products was analyzed on-line using gas chromatography fitted with flame ionization detector (FID) and thermal conductivity detector (TCD).

2.3. Characterization

N₂ adsorption–desorption isotherms were measured by Autosorb-iQ analyzer. The specific surface area was calculated by Brunauer–Emmett–Teller (BET) equation and pore size distribution was calculated by Barret–Joyner–Halenda (BJH) equation from the N₂ sorption isotherm.

X-ray diffraction (XRD) were collected on X'Pert Pro diffraction instrument using Cu K α radiation over the range 0.6° < 2θ < 5° and 5° < 2θ < 80°.

Transmission electron microscopy (TEM) images were conducted at TECNAIG² F20 instrument.

X-ray photoelectron spectroscopy (XPS) were recorded on Thermo ESCALAB 250xi spectrometer. The binding energies were calibrated against at 284.8 eV of C1s.

H₂ temperature-programmed reduction (H₂-TPR) was performed on ChemBET Pulsar Analyzer. Prior to the tests, sample was pretreated at 300 °C in He flow for 30 min. After cooling to ambient temperature, then raised temperature to 650 °C in 10% H₂–Ar mixed flow.

NH₃ temperature-programmed desorption (NH₃-TPD) was recorded on ChemBET Pulsar analyzer combining with mass spectroscopy. After being pretreated at 300 °C in He flow, the sample adsorbed NH₃ to saturation at 120 °C. The profile was detected from 50 °C to 600 °C.

Thermogravimetric-differential scanning calorimetry (TG-DSC) was based on a NETZSCH STA 449F3 analyzer under air within 20–800 °C at 10 °C min⁻¹.

The Zn content in a series of *x*Zn/Al₂O₃ catalysts were measured by inductively coupled plasma optical emission spectrometer (ICP-OES, 725-ES, Agilent).

3. Results and discussion

3.1. XRD analysis

The XRD patterns of all the as-synthesized *x*Zn/Al₂O₃ materials are presented in Fig. 1. As displayed from Fig. 1A inside, a distinct reflection peak was observed in 3–10%Zn/Al₂O₃ samples at the characteristic reflection (100) of *p6mm* space group, which confirming that these materials were composed of a well ordered mesoporous structure.²⁵ With further increasing Zn content to 15%, the diffraction peak at 0.8° became almost disappeared, indicating the significant effect of zinc content in building the ordered mesoporous structure. Part B of Fig. 1 presents the wide-angle XRD patterns of all the materials, which revealed the existence of amorphous Al₂O₃. Only the 15%Zn/Al₂O₃ sample exhibited sharp diffraction peaks associated with hexagonal crystalline ZnO (no. 89-1397 from the ICDD). The average size of these ZnO particles is 23.8 nm. On the contrary, no diffraction peaks for Zn species came into sight in 3–10%Zn/Al₂O₃ materials with ordered mesopore, implying Zn species highly dispersed on support surface or incorporated into amorphous alumina framework.²⁶ In conclusion, the presence of ordered mesoporous structure played an important role in promoting the dispersion of Zn species on the catalyst support.

3.2. Nitrogen adsorption–desorption analysis

The nitrogen adsorption–desorption analysis of all the as-synthesized *x*Zn/Al₂O₃ materials is displayed in Fig. 2. Each sample but 15%Zn/Al₂O₃ exhibited typical IV type isotherm as well as H1 shaped hysteresis loop, implying the presence of uniform cylindrical mesoporous channel in these catalysts.²⁷ Furthermore, the 3–10%Zn/Al₂O₃ samples possessed quite narrow pore size distribution around 9.5 nm, while that of 15%Zn/Al₂O₃ sample was bigger (around 12.4 nm). It suggested that the larger pores could be accumulated by ZnO particles. Table 1 listed the detailed data regarding to the textural properties of above samples. It has been observed that the specific surface area of as-synthesized 3–10%Zn/Al₂O₃ materials was similar (around 163 m² g⁻¹), which because Zn species highly dispersed on support surface or incorporated into alumina framework wouldn't lead to pore plugging. At a Zn content of 15%, the specific surface area was only 31 m² g⁻¹ owing to the mesoporous structure collapsed. It has been known that a larger surface area conduced to the better dispersion of active species, thereby can provide more "accessible" active centers for the reactant gas.²⁸ Therefore, these as-synthesized 3–10%Zn/Al₂O₃ catalysts may own preferable catalytic performance.



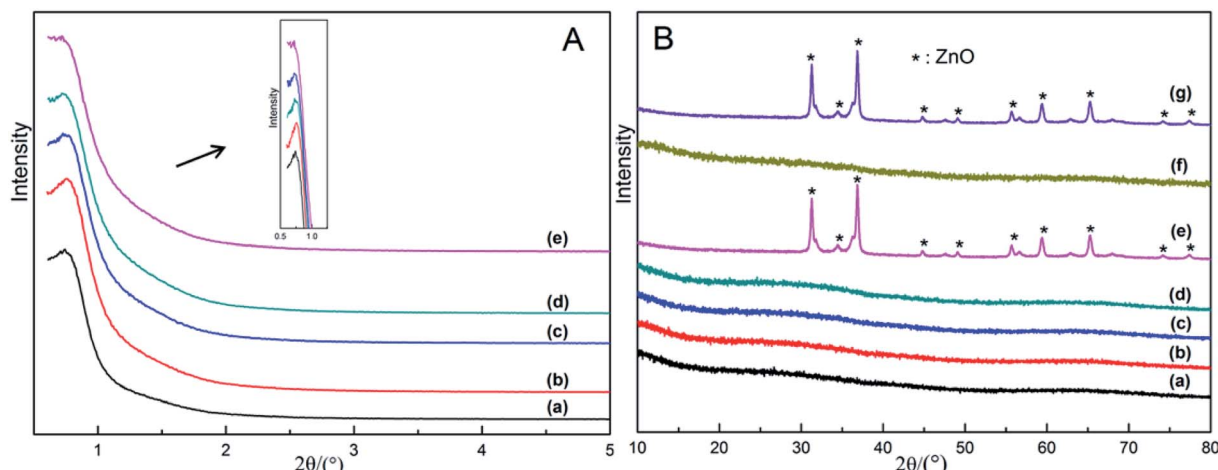


Fig. 1 The XRD patterns of the as-synthesized and spent $x\text{Zn}/\text{Al}_2\text{O}_3$ catalysts: (a) 3%Zn/Al₂O₃; (b) 5%Zn/Al₂O₃; (c) 7%Zn/Al₂O₃; (d) 10%Zn/Al₂O₃; (e) 15%Zn/Al₂O₃; (f) the spent 10%Zn/Al₂O₃; (g) the spent 15%Zn/Al₂O₃.

3.3. TEM analysis

The morphology and structure of all the as-synthesized $x\text{Zn}/\text{Al}_2\text{O}_3$ materials were performed by TEM (Fig. 3). From the images, all the sample except 15%Zn/Al₂O₃ presented one dimensional parallel channel along [1 1 0], which intuitively confirmed the presence of well-ordered mesoporous structure in the 3–10%Zn/Al₂O₃ catalysts. Notably, no distinct ZnO clusters were invisible in the images, illustrating the high dispersion of Zn species on the ordered mesoporous channel. This result conformed to the low-angle XRD analysis. Only a fraction of ordered mesopore was formed for 15%Zn/Al₂O₃ sample. In the EDX profile of 10%Zn/Al₂O₃ sample (Fig. 3f), the characteristic peaks of Al, Zn, O element can be observed clearly, which verified that Zn species had been successfully loaded. Besides, elemental mapping has further confirmed the ordered mesoporous structure and shown Zn species on the surface to be highly dispersed and distributed homogeneously over the 10%Zn/Al₂O₃ catalyst. However, an obvious aggregation of ZnO

particles was visible on the surface of 15%Zn/Al₂O₃ catalyst, which conformed the result of wide-angle XRD analysis (Fig. 4).

3.4. XPS analysis

The XPS spectra of Zn 2p orbital for all the as-synthesized $x\text{Zn}/\text{Al}_2\text{O}_3$ materials are depicted in Fig. 5. As displayed, the binding energy located at 1021.2–1201.6 eV and 1044.3–1044.7 eV was assigned to Zn²⁺, as proved by spin-orbital splitting of 23.1 eV between Zn 2p_{3/2} and Zn 2p_{1/2}.^{29,30} Noteworthy, the binding energy of Zn 2p in the sample 15%Zn/Al₂O₃ was lower than that of 10%Zn/Al₂O₃, which may be derived from the difference of Zn species in these catalysts. By deconvolution, the peak of 15%Zn/Al₂O₃ was divided into two peaks, the big one may be assigned to bulk ZnO particle on the surface, another small one may belong to Zn species incorporated into alumina framework. The Zn content calculated by XPS and ICP-OES was used to affirmed and the corresponding data listed in Table 1. We can see that the bulk Zn contents were closely to the calculated data,

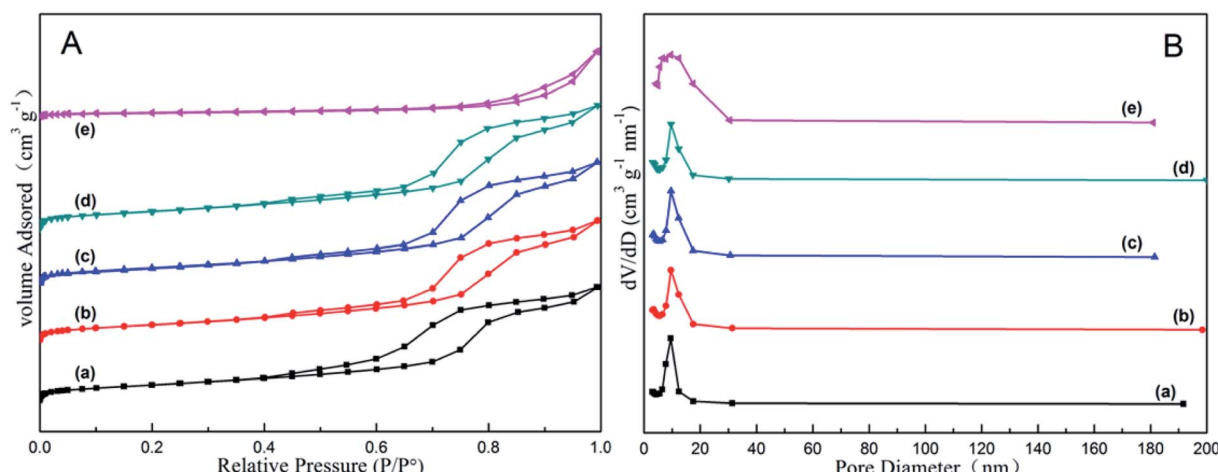


Fig. 2 The nitrogen adsorption–desorption analysis of the as-synthesized $x\text{Zn}/\text{Al}_2\text{O}_3$ catalysts: (a) 3%Zn/Al₂O₃; (b) 5%Zn/Al₂O₃; (c) 7%Zn/Al₂O₃; (d) 10%Zn/Al₂O₃; (e) 15%Zn/Al₂O₃.



Table 1 The textural data of the as-synthesized $x\text{Zn}/\text{Al}_2\text{O}_3$ catalysts^a

Samples	S_{BET} (m ² g ⁻¹)	V_p (cm ³ g ⁻¹)	d_p (nm)	Isotherm type	Zn content (%)	
					XPS	ICP-OES
3%Zn/ Al_2O_3	163.3	0.41	9.5	IV	1.6	2.5
5%Zn/ Al_2O_3	162.6	0.43	9.6	IV	2.3	4.3
7%Zn/ Al_2O_3	163.4	0.44	9.6	IV	3.0	6.4
10%Zn/ Al_2O_3	163.3	0.43	9.6	IV	3.8	9.7
15%Zn/ Al_2O_3	31.3	0.23	12.4	III	14.6	12.8
10%Zn/ $\text{Al}_2\text{O}_3^{\text{a}}$	149.7	0.40	9.3	IV	—	—
10%Zn/ $\text{Al}_2\text{O}_3^{\text{b}}$	158.6	0.42	9.5	IV	—	—
15%Zn/ $\text{Al}_2\text{O}_3^{\text{a}}$	25.2	0.16	11.8	III	—	—

^a ^b Stand for the corresponding spent and fifth regenerated catalyst, respectively.

only 15%Zn/ Al_2O_3 had a larger deviation. Moreover, the surface Zn content (14.6%) of this sample from XPS was higher than the actual Zn content (12.8%), suggesting aggregation of ZnO

particles on the surface. In contrast, the surface Zn was less than the bulk for 3–10%Zn/ Al_2O_3 samples, which was due to most of Zn species incorporated into alumina framework. These

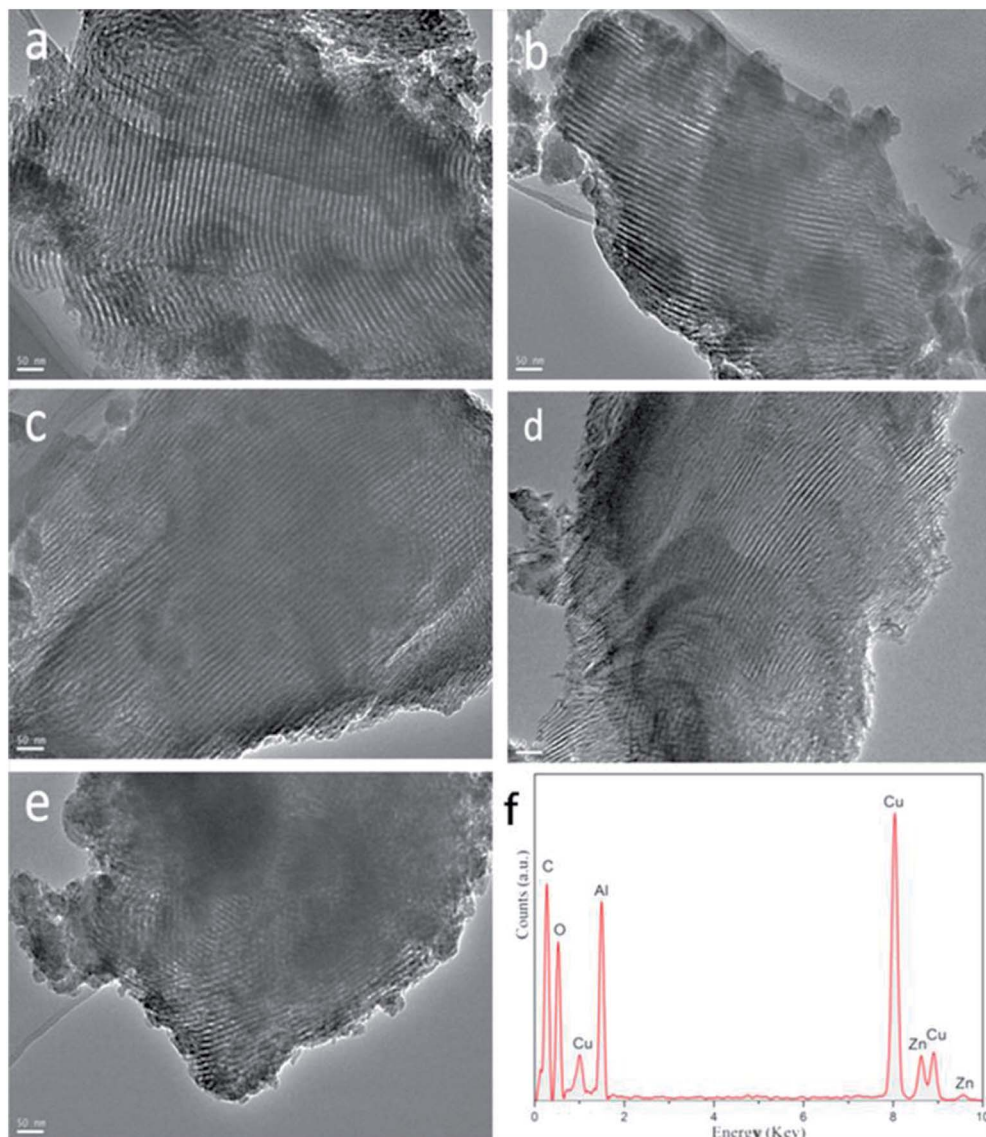


Fig. 3 The TEM images of the as-synthesized $x\text{Zn}/\text{Al}_2\text{O}_3$ catalysts: (a) 3%Zn/ Al_2O_3 ; (b) 5%Zn/ Al_2O_3 ; (c) 7%Zn/ Al_2O_3 ; (d) 10%Zn/ Al_2O_3 ; (e) 15%Zn/ Al_2O_3 . (f) EDX characterization for 10%Zn/ Al_2O_3 .



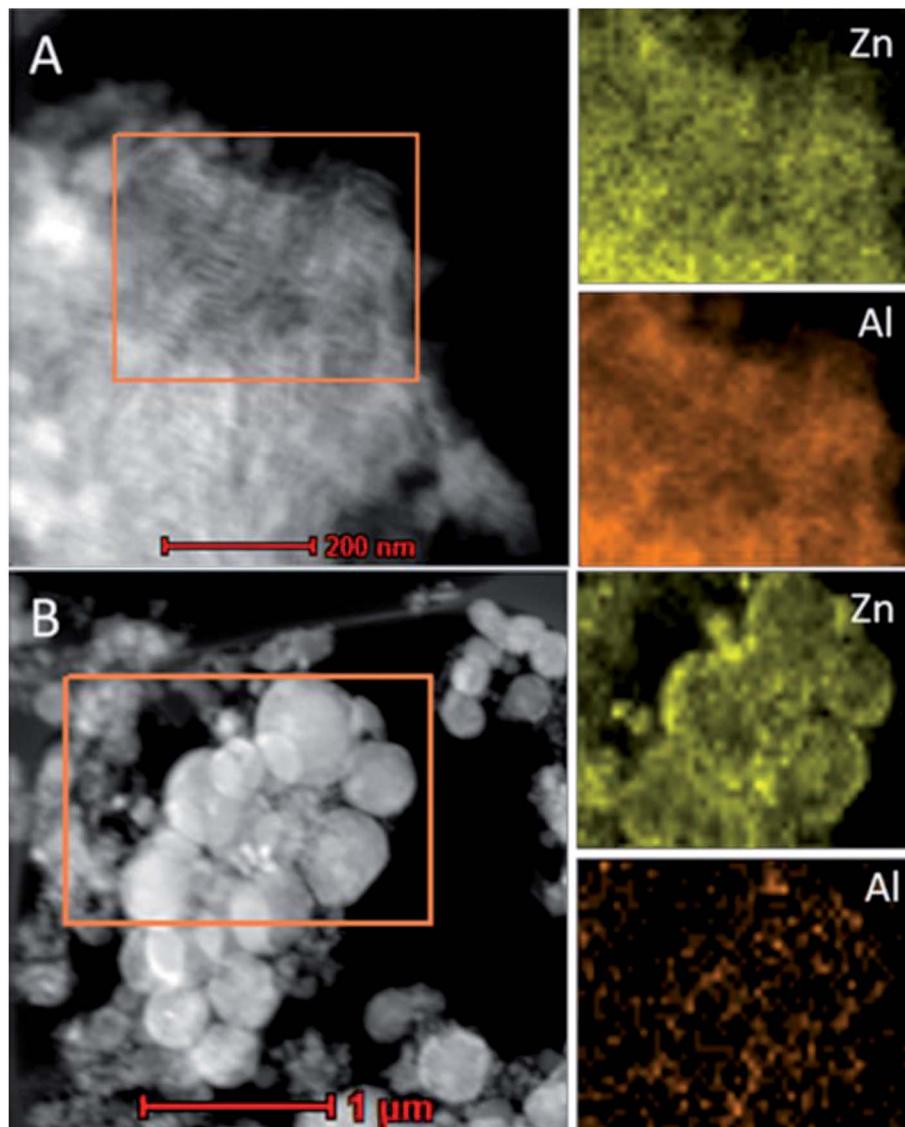


Fig. 4 TEM image and Zn, Al elemental mappings of the fresh samples: (A) 10%Zn/Al₂O₃; (B) 15%Zn/Al₂O₃.

results were accorded with wide-angle XRD analysis and confirmed the change of Zn species when increased Zn content from 10% to 15%. Besides, the higher binding energy meaning a stronger interaction between Zn species and support in 3–10% Zn/Al₂O₃ catalysts. This result will be further confirmed by following H₂-TPR characterization.

3.5. H₂-TPR profiles

H₂-TPR characterization is a very useful instrument to investigate the interaction between Zn species and catalyst support. The results for the as-synthesized x Zn/Al₂O₃ materials and pure ZnO are shown in Fig. 6. All profiles of x Zn/Al₂O₃ showed a broad reduction peak around 490 °C, which could be assigned to the reduction of highly dispersed zinc species on support surface and Zn species incorporated into alumina framework. However, 15%Zn/Al₂O₃ catalyst presented a unique reduction peak at 416 °C, which was similar with the reduction peak of

pure bulk ZnO. More specifically, this peak belonged to the reduction of binuclear (Zn–O–Zn)²⁺ clusters.³¹ It has been known that the higher reduction temperature, the stronger interaction between metal and support. Therefore, the Zn species with the reduction peak around 490 °C have stronger interaction with support.³² The characterization of H₂-TPR was coincided with the above XRD and XPS analysis.

3.6. NH₃-TPD analysis

The acidic property of all the as-synthesized x Zn/Al₂O₃ materials was determined by NH₃-TPD and the corresponding results are displayed in Fig. S1.† All the samples exhibited a broad peak at 50–600 °C, indicating abundant different intensities of acidic sites in x Zn/Al₂O₃ catalysts. By deconvolution, the broad peak was divided into four peaks accredited to physically adsorbed NH₃, weak, medium and strong acidic sites respectively.^{33,34} The detailed calculation result was in Table 2. As displayed, all the



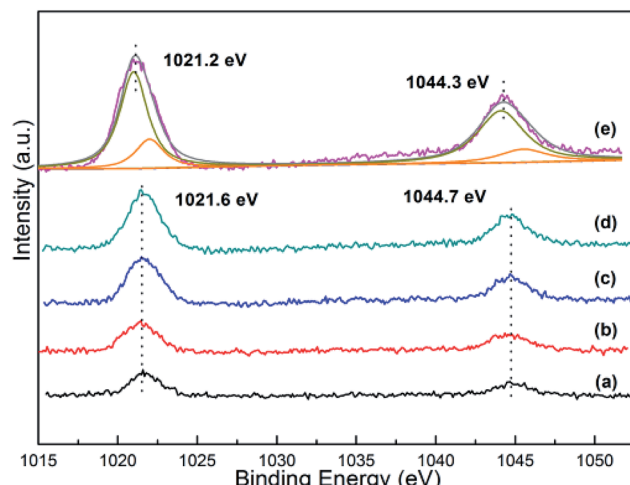


Fig. 5 The Zn 2p XPS spectra of the as-synthesized $x\text{Zn}/\text{Al}_2\text{O}_3$ catalysts: (a) 3% $\text{Zn}/\text{Al}_2\text{O}_3$; (b) 5% $\text{Zn}/\text{Al}_2\text{O}_3$; (c) 7% $\text{Zn}/\text{Al}_2\text{O}_3$; (d) 10% $\text{Zn}/\text{Al}_2\text{O}_3$; (e) 15% $\text{Zn}/\text{Al}_2\text{O}_3$.

samples except for 15% $\text{Zn}/\text{Al}_2\text{O}_3$ exhibited similar amount of physically adsorbed NH_3 , which due to their comparable pore property. However, the specific surface area and pore volume of

15% $\text{Zn}/\text{Al}_2\text{O}_3$ was much smaller, then physically adsorbed NH_3 also less than other samples. Besides, we can see that there are three different acidic sites on pure ordered mesoporous Al_2O_3 . With the introduction of 3%Zn, the amount of three acidic sites significantly enhanced. It indicated that a part of three types acid sites originated from surface hydroxyl group and coordinative unsaturated Al sites on Al_2O_3 support, and other derived from Zn species.^{15,35} Note that the total and weak acidic sites gradually increased, while the strong acidic sites decreased slowly with the increase of Zn content until 10%. When the Zn content reached 15%, the total acidic strength of this catalyst declined sharply, which may due to bulk ZnO has rarely acidic sites (Fig. S2†). It was well established that weak and medium acid sites played a key role to isobutane conversion in dehydrogenation reaction.¹⁵ However, side reactions (polymerization, isomerization and cracking) are mainly catalyzed by strong acid sites.³⁶ As a conclusion, the various $x\text{Zn}/\text{Al}_2\text{O}_3$ catalysts with the different number of acidic sites may present distinct catalytic performance.

3.7. Catalytic performance in the isobutane dehydrogenation

The reactivity of isobutane dehydrogenation over a series of $x\text{Zn}/\text{Al}_2\text{O}_3$ catalysts is displayed in Fig. 7. As we can notice that the catalytic activity of $x\text{Zn}/\text{Al}_2\text{O}_3$ catalysts gradually increased until 10% Zn content. The 10% $\text{Zn}/\text{Al}_2\text{O}_3$ catalyst exhibited a notably higher initial isobutane conversion (46.6%) and initial isobutene selectivity (81.8%) by contrast with the 3% $\text{Zn}/\text{Al}_2\text{O}_3$ (29.4% conversion and 69.4% selectivity), indicating that Zn content was a very significant factor in isobutane dehydrogenation reaction. In addition to this, with increasing reaction time, the reactivity over the 3–10% $\text{Zn}/\text{Al}_2\text{O}_3$ catalysts can basically hold steady, while the 15% $\text{Zn}/\text{Al}_2\text{O}_3$ catalyst presented poor catalytic stability.

Isobutane dehydrogenation is an endothermic reaction in thermodynamics, which need relatively high temperature to obtain excellent isobutene yield. The effect of reaction temperature on catalytic activity of 10% $\text{Zn}/\text{Al}_2\text{O}_3$ catalyst was investigated in Fig. 8. The conversion of isobutane was 45.0% and the selectivity of isobutene was 86.7% at 580 °C after 30 min. With the increase of the reaction temperature, the conversion of isobutane obviously increased and selectivity of isobutene significantly decreased, which was quite conformed to the characteristic of alkane dehydrogenation reaction. However, the

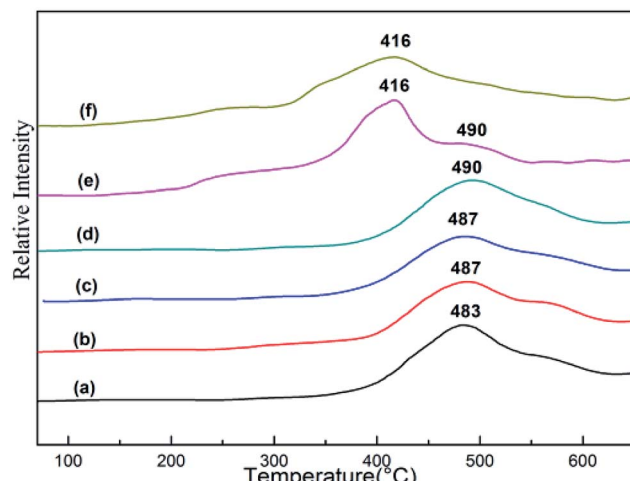


Fig. 6 The H_2 -TPR profiles of the as-synthesized $x\text{Zn}/\text{Al}_2\text{O}_3$ catalysts: (a) 3% $\text{Zn}/\text{Al}_2\text{O}_3$; (b) 5% $\text{Zn}/\text{Al}_2\text{O}_3$; (c) 7% $\text{Zn}/\text{Al}_2\text{O}_3$; (d) 10% $\text{Zn}/\text{Al}_2\text{O}_3$; (e) 15% $\text{Zn}/\text{Al}_2\text{O}_3$; (f) ZnO .

Table 2 The acidic properties of the as-synthesized Al_2O_3 and $x\text{Zn}/\text{Al}_2\text{O}_3$ catalysts

Samples	Physically adsorbed NH_3 (mmol g ⁻¹)	The amount of acidic sites (mmol g ⁻¹)			
		Weak	Medium	Strong	Total
Al_2O_3	0.007	0.037	0.021	0.009	0.067
3% $\text{Zn}/\text{Al}_2\text{O}_3$	0.008	0.048	0.051	0.026	0.125
5% $\text{Zn}/\text{Al}_2\text{O}_3$	0.009	0.061	0.043	0.024	0.128
7% $\text{Zn}/\text{Al}_2\text{O}_3$	0.010	0.066	0.041	0.023	0.130
10% $\text{Zn}/\text{Al}_2\text{O}_3$	0.009	0.069	0.048	0.016	0.133
15% $\text{Zn}/\text{Al}_2\text{O}_3$	0.004	0.036	0.033	—	0.069

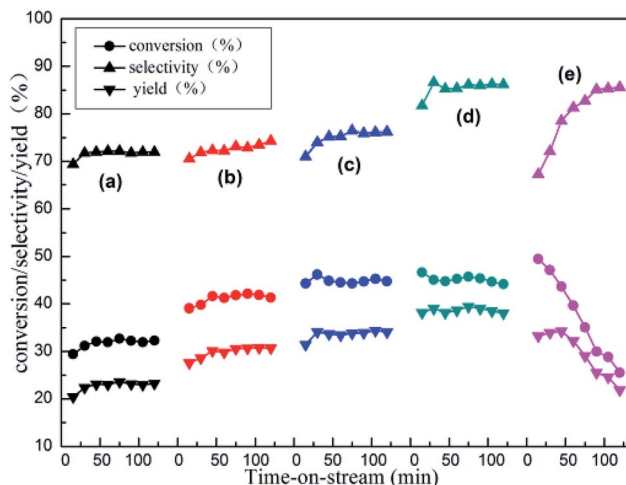


Fig. 7 The reactivity of isobutane dehydrogenation over the as-synthesized $x\text{Zn}/\text{Al}_2\text{O}_3$ catalysts: (a) 3%Zn/Al₂O₃; (b) 5%Zn/Al₂O₃; (c) 7%Zn/Al₂O₃; (d) 10%Zn/Al₂O₃; (e) 15%Zn/Al₂O₃. Reaction condition: $T = 580\text{ }^\circ\text{C}$, GHSV = 300 h^{-1} .

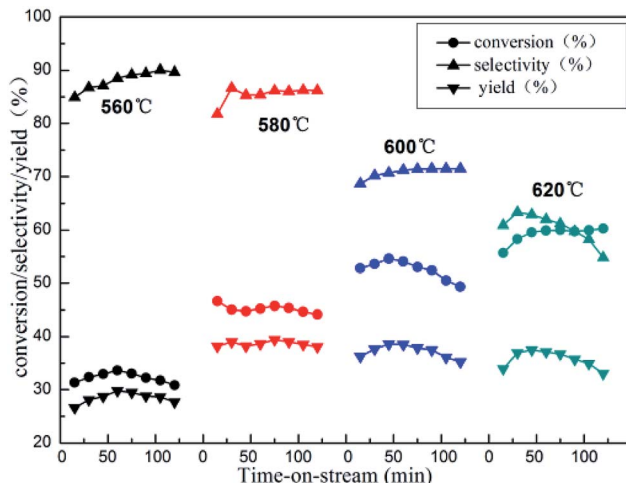


Fig. 8 The reactivity of isobutane dehydrogenation over the 10%Zn/Al₂O₃ catalyst. Reaction condition: GHSV = 300 h^{-1} .

isobutane conversion dropped drastically, isobutene selectivity just increased slightly with the reaction temperature decreased to 560 °C. In view of catalytic stability, 580 °C was deemed as the optimal reaction temperature.

The impact of the GHSV on catalytic activity was also carefully studied over 10%Zn/Al₂O₃ catalyst (Fig. 9). As we can see, with GHSV increasing from 300 to 600 h^{-1} , the initial isobutane conversion decreased obviously (from 46.6% to 30.6%), while initial isobutene selectivity increased (from 81.8% to 91.1%). As the GHSV continues to rise, it became slope that isobutane conversion decreased with time on stream.

In order to further investigate what were active sites for isobutane dehydrogenation, we tested this reaction at 580 °C over ordered mesoporous Al₂O₃ and commercial ZnO as a contrast (Fig. S3†). It can be seen that initial isobutane

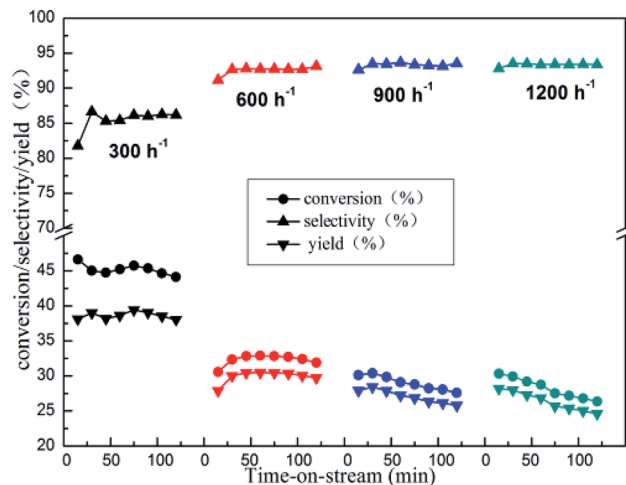


Fig. 9 The reactivity of isobutane dehydrogenation over the 10%Zn/Al₂O₃ catalyst. Reaction condition: $T = 580\text{ }^\circ\text{C}$.

conversion and initial isobutene yield over Al₂O₃ were only 3.1% and 2.1%, which illustrated that ordered mesoporous Al₂O₃ was inactive to the reaction. ZnO exhibited slightly higher initial dehydrogenation activity (9.2% isobutane conversion and 5.5% isobutene yield). It seemed that bulk ZnO particle had some catalytic ability. Surprisingly, with the introduction of Zn, the $x\text{Zn}/\text{Al}_2\text{O}_3$ catalysts exhibited very excellent initial catalytic activity, even then the ordered mesopore collapsed and Zn species was not highly dispersed over 15%Zn/Al₂O₃ catalyst. Considering the possibility of zinc incorporated into Al₂O₃ framework over 15%Zn/Al₂O₃ catalyst, we deduced that the existence of framework zinc may play a crucial role. However, there is no direct evidence for this. The essential role of Zn species of $x\text{Zn}/\text{Al}_2\text{O}_3$ in isobutane dehydrogenation still need to be identified, which is the focus of the following work in our laboratory. In addition, it is well-known that the amount of different acidic sites of catalyst are the key to affect catalytic activity in alkane dehydrogenation reaction.³⁷ The isobutane

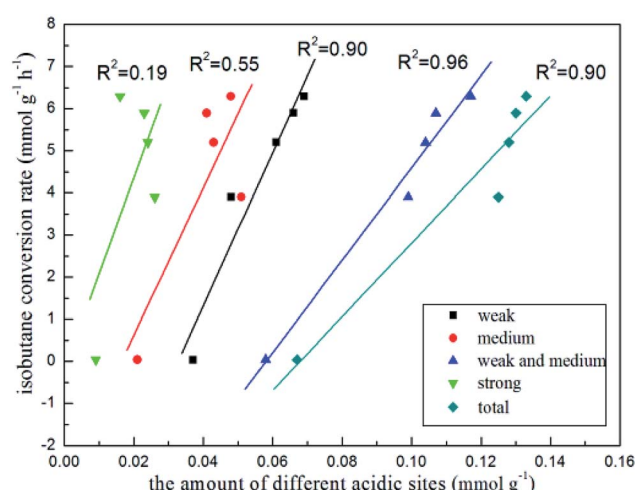


Fig. 10 The trend of isobutane conversion rate with the amount of different kinds of the acidic sites.

conversion rate *vs.* the number of different acidic sites on the basis of Table 2 were plotted (Fig. 10). The isobutane conversion rate *versus* the amount of strong acidic sites showed the worst linear correlation ($R^2 = 0.19$), nevertheless, *versus* the amount of weak and medium acidic sites presented the best linear correlation ($R^2 = 0.96$), indicating that strong acidic sites were not the decisive factor for isobutane conversion, while both the weak and medium acidic sites took the important part in isobutane conversion. Besides, the isobutane selectivity was obviously increased with the decrease of the amount of strong acidic sites over 3–10%Zn/Al₂O₃ catalysts, indicated strong acid sites mainly catalyzed side reactions.

3.8. The stability of ordered mesoporous Zn/Al₂O₃ catalyst

3.8.1. XRD analysis. The wide-angle XRD patterns of the spent catalysts are shown in Fig. 1. It was observed that there is

no difference between fresh and spent catalysts. The crystalline ZnO phase was also visible over spent 15%Zn/Al₂O₃ catalyst, and no Zn species over the spent 10%Zn/Al₂O₃ catalyst as well, indicating that Zn species were stable without phase transformation during this dehydrogenation reaction.

3.8.2. Nitrogen adsorption–desorption analysis. The nitrogen adsorption–desorption analysis of the spent and regenerated catalysts are in Fig. S4.† Compared with the corresponding fresh catalysts, the isotherms of spent catalysts had no obvious changed and still presented uniform pore size. The textural properties are presented in Table 1. It was clearly seen that the BET specific surface areas of the spent 10%Zn/Al₂O₃ and 15%Zn/Al₂O₃ catalysts were greatly reduced to 149.7 m² g⁻¹ and 25.2 m² g⁻¹, respectively. It was probably due to that coke deposition on the spent catalyst blocked a portion of the pore, thus leading to the decrease of textural performance. After five dehydrogenation–regeneration cycles, the slightly diminished

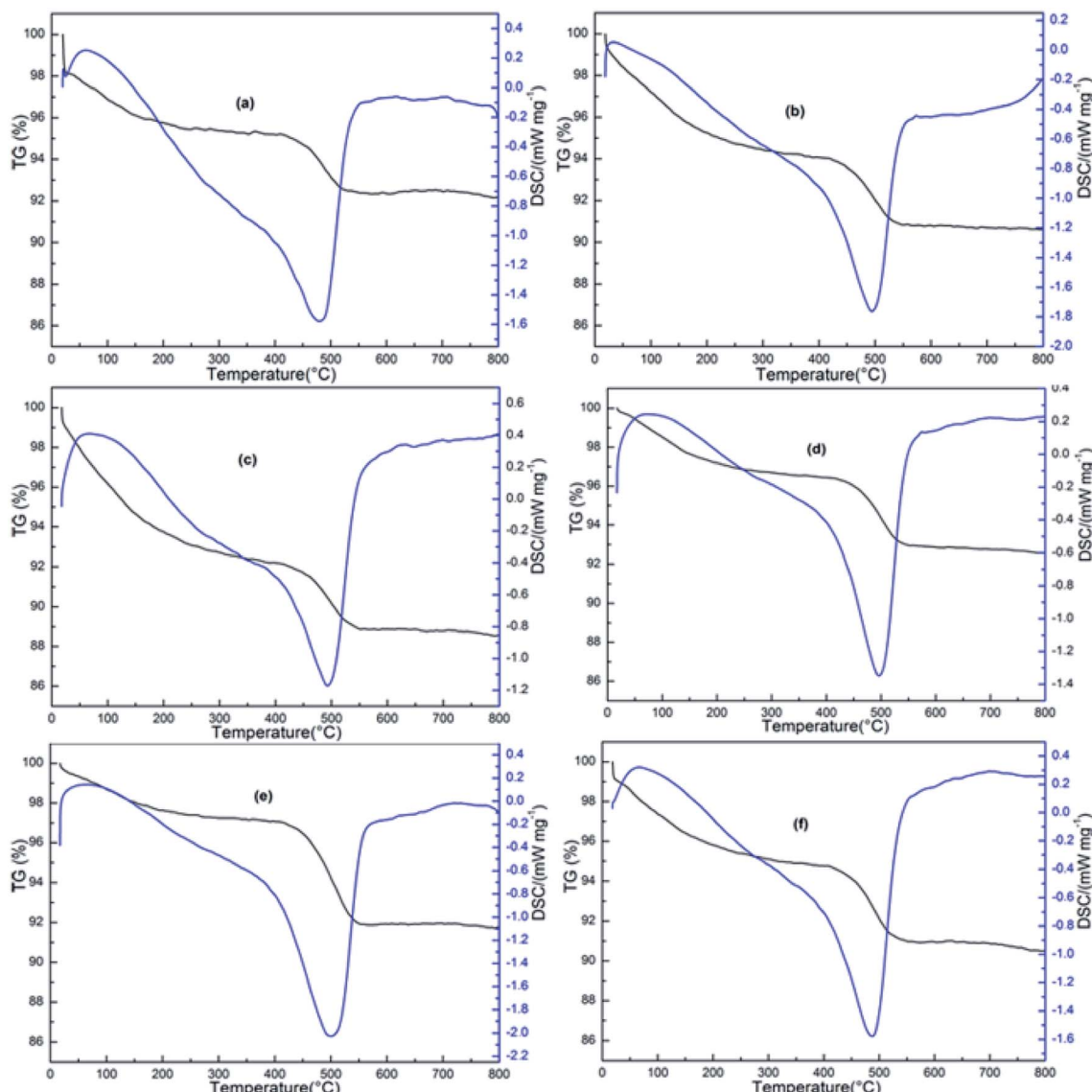


Fig. 11 TG-DSC curves of the spent catalysts at 580 °C reaction: (a) 3%Zn/Al₂O₃; (b) 5%Zn/Al₂O₃; (c) 7%Zn/Al₂O₃; (d) 10%Zn/Al₂O₃; (e) 15%Zn/Al₂O₃ and the spent catalyst at 620 °C reaction: (f) 10%Zn/Al₂O₃.

specific surface area ($163.3 \rightarrow 158.6 \text{ m}^2 \text{ g}^{-1}$) and pore volume ($0.43 \rightarrow 0.42 \text{ cm}^3 \text{ g}^{-1}$) of the regenerated 10%Zn/Al₂O₃ demonstrated the formed coke can be eliminated by regeneration process.

3.8.3. TG-DSC analysis. As we all know, coking is usually the main reason for catalyst deactivation in alkane dehydrogenation reaction. TG-DSC is a very efficient technique to analyze the coke amount and the characterization results are shown in Fig. 11. The TG curves presented downtrend with the increase of temperature, which could be divided into two stages. In the first stage, the weight losses in TG curves up to 300 °C, ascribed to the loss of physically adsorbed water and impurities. The second stage, located in the 350–600 °C, the losses was assigned to the removal of coke. The coke amount in the spent 3%Zn/Al₂O₃, 5%Zn/Al₂O₃, 7%Zn/Al₂O₃ and 10%Zn/Al₂O₃ were 2.97%, 3.22%, 3.29% and 3.45%, respectively. Which similar coke amount was consistent with the same good stability of these ordered mesoporous catalysts. However, with increasing Zn content to 15%, coke amount was markedly increased (5.19%). Combined with the poor stability of 15%Zn/Al₂O₃ catalyst, the reason of serious deactivation may caused by more coke, which also indicated ordered meso-structure could effectively inhibited the formation of coke.³⁸ Moreover, during 620 °C reaction temperature, the coke amount in the spent 10%Zn/Al₂O₃ catalyst increased to 3.79%. It explained the stability decreased with the increase of reaction temperature.

3.8.4. The dehydrogenation–regeneration cycles. In order to examine the regenerative ability of the 10%Zn/Al₂O₃ catalyst, the five dehydrogenation–regeneration cycles were investigated (Fig. 12). By calculation, the initial isobutane conversion, isobutene selectivity and yield were 45.1%, 83.6% and 37.7% in the first cycle, respectively. With increasing reaction time, the catalytic activity decreased gradually. Following by 2 h regeneration of catalyst at 600 °C in air, the activity of catalyst was obviously restored, which affirmed coke was the main reason of catalyst deactivation. In the five cycle, the initial isobutane

conversion, isobutene selectivity and yield were decrease slightly, indicated the high regenerative ability of the catalyst.

4. Conclusions

A series of x Zn/Al₂O₃ materials with various Zn content were simply prepared *via* one pot EISA strategy and tested in isobutane dehydrogenation reaction. The obtained materials with Zn content up to 10% possessed well-ordered mesopore with large specific surface areas, big pore volumes and uniform pore size. Zinc species in these catalysts was highly dispersed on support surface or incorporated into framework, while ZnO crystal particles were observed with 23.8 nm size in the case of 15%Zn. It was found that these materials presented excellent catalytic activity. Note that the total acidic sites gradually increased, while the strong acidic sites decreased slowly with the increase of Zn content until 10%. The decrease of strong acid sites is conducive to the promotion of isobutene selectivity and the weak and medium acidic sites played a role in isobutane conversion. In addition, the catalyst exhibited excellent stability and high regenerative ability, which demonstrated potential for commercial applications.

Conflicts of interest

There are no conflicts to declare.

Acknowledgements

The authors sincerely acknowledge the financial support from the National Natural Science Foundation of China (no. 21573260 and No. 21403255), Youth Innovation Promotion Association CAS (no. 2017460) and Jiangsu Science and Technology Program (no. BY2016048-01).

References

1. I. Gniot, P. Kirszensztein and M. Kozłowski, *Appl. Catal., A*, 2009, **362**, 67–74.
2. A. Feller, I. Zuazo, A. Guzman, J. O. Barth and J. A. Lercher, *J. Catal.*, 2003, **216**, 313–323.
3. Y. Tian, X. Liu, M. Rood and Z. Yan, *Appl. Catal., A*, 2017, **41**, 1–9.
4. S. Al-Zahran, N. Elbashir, A. Abasaed and M. Abdulwahed, *Ind. Eng. Chem. Res.*, 2001, **40**, 781–784.
5. L. Wan, Y. Zhou, Y. Zhang, Y. Duan, X. Liu and M. Xue, *Ind. Eng. Chem. Res.*, 2011, **58**, 4280–4285.
6. J. Zhang, D. Su, A. Zhang, D. Wang, R. Schlögl and C. Hebert, *Angew. Chem., Int. Ed.*, 2007, **46**, 7319–7323.
7. J. Grant, C. Carrero, F. Goeltl, J. Venegas, P. Mueller, S. Burt, S. Specht, W. McDermott, A. Chieregato and I. Hermans, *Science*, 2016, **354**, 1570–1573.
8. J. H. B. Sattler, J. Ruiz-Martinez, E. Santillan-Jimenez and B. M. Weckhuysen, *Chem. Rev.*, 2014, **114**, 10613–10653.
9. J. Mu, J. Shi, L. France, Y. Wu, Q. Zeng, B. Liu, Li. Jiang, J. Long and X. Li, *ACS Appl. Mater. Interfaces*, 2018, **10**, 23112–23121.

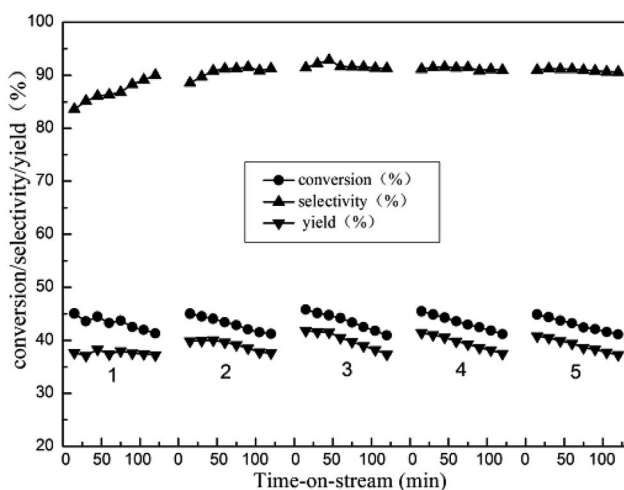


Fig. 12 The five dehydrogenation–regeneration cycles of isobutane dehydrogenation over 10%Zn/Al₂O₃ catalyst. Reaction condition: $T = 580 \text{ }^{\circ}\text{C}$, GHSV = 300 h⁻¹.



10 H. Zhao, H. Song, J. Yang, J. Zhao, L. Yan and L. Chou, *Catal. Sci. Technol.*, 2017, **15**, 3256–3267.

11 S. Wang, K. Wang and X. Wang, *Appl. Surf. Sci.*, 2016, **386**, 442–450.

12 M. Cheng, H. Zhao, J. Yang, J. Zhao, L. Yan, H. Song and L. Chou, *Microporous Mesoporous Mater.*, 2018, **266**, 117–125.

13 J. Liu, A. Hong, N. He, G. Liu, C. Liang, X. Zhang and H. Guo, *Chem. Eng. J.*, 2013, **218**, 1–8.

14 Y. Sun and T. Brown, *Int. J. Chem. Kinet.*, 2002, **34**, 467–480.

15 G. Liu, J. Liu, N. He, C. Miao, J. Wang, Q. Xin and H. Guo, *RSC Adv.*, 2018, **8**, 18663–18671.

16 Z. Chen, A. Derking, W. Koot and M. van Dijk, *J. Catal.*, 1996, **161**, 730–741.

17 G. Wang, C. Li and H. Shan, *Catal. Sci. Technol.*, 2016, **6**, 3128–3136.

18 W. Wang, K. Zhang, Y. Yang, H. Liu, Z. Qiao and H. Luo, *Microporous Mesoporous Mater.*, 2014, **193**, 47–53.

19 S. M. Morris, P. F. Fulvio and M. Jaroniec, *J. Am. Chem. Soc.*, 2008, **130**, 15210–15216.

20 Q. Yuan, A. Yin, C. Luo, L. Sun, Y. Zhang, W. Duan, H. Liu and C. Yan, *J. Am. Chem. Soc.*, 2008, **130**, 3465–3472.

21 N. M. Schweitzer, B. Hu, U. Das, H. Kim and A. S. Hock, *ACS Catal.*, 2014, **4**, 1091–1098.

22 L. Xu, Z. Wang, H. Song and L. Chou, *Catal. Commun.*, 2013, **35**, 76–81.

23 M. Morris, P. Fulvio and M. Jaroniec, *J. Am. Chem. Soc.*, 2008, **130**, 15210–15216.

24 L. Xu, H. Song and L. Chou, *Int. J. Hydrogen Energy*, 2013, **38**, 7307–7325.

25 D. Pan, W. Chen, F. Yu, S. Chen, X. Yan, X. Shi, B. Fan and R. Li, *Mater. Lett.*, 2018, **224**, 33–36.

26 X. Xiang, H. Zhao, J. Yang, J. Zhao, L. Yan, H. Song and L. Chou, *Appl. Catal. A*, 2016, **520**, 140–150.

27 M. Kruk and M. Jaroniec, *Chem. Mater.*, 2001, **13**, 3169–3183.

28 Z. He, Y. Jiao, J. Wang and Y. Chen, *Fuel*, 2018, **212**, 193–201.

29 A. Choi, J. Park, Y. Kang, S. Lee and Y. Kang, *Phys. B*, 2018, **537**, 251–257.

30 W. Gu, X. Wu and J. Zhang, *Mater. Sci. Semicond. Process.*, 2018, **81**, 89–93.

31 S. Tamiyakul, W. Ubolcharoen, D. N. Tungasmita and S. Jongpatiwut, *Catal. Today*, 2015, **256**, 325–335.

32 C. Yu, H. Xu, Q. Ge and W. Li, *J. Mol. Catal. A: Chem.*, 2007, **266**, 80–87.

33 H. Ham, M. H. Jeong, H. M. Koo, C. H. Chung and J. W. Bae, *React. Kinet., Mech. Catal.*, 2015, **116**, 173–189.

34 U. Rodemerck, E. V. Kondratenko, T. Otroshchenko and D. Linke, *Chem. Commun.*, 2016, **52**, 12222–12225.

35 S. Zhang, Y. Zhou, Y. Zhang and L. Huang, *Catal. Lett.*, 2010, **135**, 76–82.

36 Y. Ren, F. Zhang, W. Hua, Y. Yue and Z. Gao, *Catal. Today*, 2009, **148**, 316–322.

37 M. Dixit, P. Kostetskyy and G. Mpourmpakis, *ACS Catal.*, 2018, **8**, 11570–11578.

38 L. Xu, Z. Miao, H. Song, W. Chen and L. Chou, *Catal. Sci. Technol.*, 2014, **4**, 1759–1770.

